INTERNATIONAL JOURNAL FOR NUMERICAL METHODS IN FLUIDS
Int. J. Numer. Meth. Fluids **28**: 887–902 (1998)

A SPECTRAL METHOD FOR FREE SURFACE FLOWS OF INVISCID FLUIDS

MIN-JOON KIM[b,*], HIE-TAE MOON[a], YONG-BUM LEE[b], SEOK-KI CHOI[b], YONG-KYUN KIM[b], HO-YUN NAM[b] AND MANN CHO[b]

[a] *Physics Department, Korea Advanced Institute of Science and Technology, Daeduk Science Town, 305-701 Daejon, Republic of Korea*
[b] *Korea Atomic Energy Research Institute, Daeduk Science Town, Daejon 305-353, Republic of Korea*

SUMMARY

In this paper, an efficient numerical method for unsteady free surface motions, with simple geometries, has been devised. Under the potential flow assumption, the governing equation of free surface flows becomes a Laplace equation, which is treated here by means of a series expansions of the velocity potential. The free surface is represented with a height function. The present method is applied to surface gravity waves to test the stability and accuracy of the method. To show the versatility of the method, a model for a dip formation is considered. © 1998 John Wiley & Sons, Ltd.

KEY WORDS: potential flow; free surface; spectral method; surface gravity waves; dip formation

1. INTRODUCTION

In developing a numerical method, there are some checkpoints, such as accuracy, speed, flexibility, versatility and so on, to consider. Among these checkpoints, the developers sometimes forget the importance of convenience of implementation. Building up a versatile and accurate method is very important. Building up a method that can be easily applied is also necessary. Complex phenomena can be frequently explained by simplified models. Even if the simplified models fail in explaining the whole phenomena, they often succeed in explaining the major phenomena. For the solutions of the simplified models, there is no need to use a general, but complicated, method. To use a simple method for a simplified model is often more efficient than using a general method for the original system. In this paper, a simple method that can be easily applied, is proposed.

The system considered is free surface flows. The phenomena of free surface motions are abundant in nature. Unfortunately, it is very difficult to study the dynamics because of the non-linearity of fluid and the existence of free surfaces, freely moving and arbitrarily shaped boundaries across which, some physical quantities vary discontinuously.

Generally, Navier–Stokes equation must be solved, which is usually hard even for fixed and simple boundaries. In this case, there is the volume of fluid (VOF) method [1,2], the markers and cell (MAC) method [3–8], and so on [9–11]. Boundary fitted co-ordinates are sometimes

* Correspondence to: KALIMER Sodium Experimental Technology Development, Korea Atomic Energy Research Institute, Daeduk Science Town, 305-353 Daejon, Republic of Korea. Fax: +82 42 8688739; e-mail: koma@hplmr01.kaeri.re.kr

CCC 0271–2091/98/160887–16$17.50

Received January 1997
Revised September 1997

used [12–18]. In many cases, it is enough to treat the flow as a potential flow. Under the assumption of the potential flow, the governing equation can be simplified to a Laplace equation, which can be handled more easily than the Navier–Stokes equation. In this case, the boundary integral method [19–21] and the vortex sheet method [22–27] are frequently used.

Since the purpose is to develop a simple numerical method for free surface flows, the potential flow assumption is adopted. The numerical method is based on a kind of series expansion that is similar to the Stokes expansion [28–30]. This kind of approach is simple, easy to implement and it is easy to interpret the results. A series expansion of the velocity potential has often been used for the study of the 'steady' free surface flows [29–35]. In this paper, the 'unsteady' free surface motions are focused upon. As far as is known, there are few examples that apply the series expansion to unsteady free surface flow calculations, directly.

To examine the accuracy and stability of the present method, surface gravity waves [28,36] are considered as a test problem. Surface gravity waves with a small amplitude is a trivial test example, but if the amplitude becomes larger, the problem becomes more difficult, with increasing non-linearity. After confirming the validity of the numerical method, the present method is applied to a dip formation problem due to a sink [21,37–41], which can be an interesting and important example.

In Section 2, the governing equations and boundary conditions for free surface flows are derived under the assumption of a potential flow. In Section 3, the numerical method employed here is explained and its characteristics discussed. In Section 4, surface gravity waves are studied with the present numerical method. By comparing the results with other results reported earlier, the accuracy and stability of the present method are discussed. In Section 5, a sink flow is studied with the present method. The study can be one example that shows the applicability of the method.

2. GOVERNING EQUATIONS

Assuming a potential flow, a non-rotational flow of an inviscid fluid, a velocity potential ϕ can be defined as

$$\vec{v} = \nabla\phi, \tag{1}$$

where $\vec{v}$ denotes velocity. The incompressibility condition gives the following Laplace equation as the governing equation,

$$\nabla^2\phi = 0. \tag{2}$$

With the appropriate boundary conditions, a full set of governing equations describing free surface flows is possible. Two kinds of boundaries need to be considered: fixed boundaries for walls and bottoms, and freely moving boundaries for free surfaces. The boundary conditions for fixed boundaries are the same as those of other fluid problems without free surfaces. That is, for an impermeable boundary, the boundary condition is

$$\hat{n} \cdot \nabla\phi = 0, \tag{3}$$

where $\hat{n}$ is the normal vector of the boundary.

For the boundary conditions at the free surface, two boundary conditions, namely, the kinematic boundary condition and the dynamic boundary condition [28] need to be considered. The kinematic boundary condition treats the fact that fluid particles, once at the free surface, must remain at the free surface. In other words, the free surface moves with the velocity of the fluid. This condition is written as

$$f_t + uf_x + vf_y + wf_z = 0 \quad \text{on } f(x, y, z, t) = 0, \tag{4}$$

where $f(x, y, z, t) = 0$ is the equation of the free surface position. Subscripts denote partial derivatives with respect to themselves and u, v, and w are, respectively, the x-, y-, and z-directional velocities.

For an inviscid fluid, the dynamic boundary condition refers to the pressure continuity condition through the free surface [5,42], which is obtained from the momentum equation at the free surface. Assuming the atmospheric pressure to be zero, the dynamic boundary condition for free surface flows under gravity is

$$\phi_t + \frac{1}{2}|\nabla\phi|^2 + gz = 0 \quad \text{on } f(x, y, z, t) = 0. \tag{5}$$

Gravitational acceleration is denoted by g, with its direction in the $-z$-direction. If there are other components, e.g. surface tension effects, Equation (5) needs to be modified.

3. NUMERICAL METHOD

Numerical methods for free surface flow calculations are composed of two main parts. One part is about representing the location of the free surface and the other is about solving the governing equations.

A free surface can be written formally as $z = \eta(x, y, t)$. Here, η is sometimes called the 'height function'. The height function representation, while it is very simple, has some limitations. One major limitation is that the height function method can not describe multivalued surface profiles. For example, it is hard to apply the height function method to wave breaking phenomena. Another shortcoming of the height function method is faced when one tries to solve the governing equations. Usually, the height function approach produces large errors at the points on which the derivative of the height function, the slope of the free surface, is greater than the grid resolution, say $\delta z/\delta x$ [1], with δx and δz being the grid sizes in the x- and z-directions, respectively. In spite of these shortcomings, the height function method is still useful and powerful for the free surface flow calculations due to its simplicity.

The method for the governing equations will be discussed now. Under the potential flow assumption, the governing equations are reduced, through the introduction of a velocity potential ϕ, to a Laplace equation with proper boundary conditions. Then, the major point to free surface flow calculations becomes how to efficiently solve the Laplace equation under the kinematic and dynamic boundary conditions. To discuss the method employed in this paper, the governing equations and the boundary conditions with a height function and a velocity potential, will be discussed first.

$$\nabla^2\phi = 0, \tag{6}$$

$$\eta_t + \phi_x\eta_x + \phi_y\eta_y = \phi_z \quad \text{on } \eta(x, y, t), \tag{7}$$

$$\phi_t + \frac{1}{2}|\nabla\phi|^2 + gz = 0 \quad \text{on } z = \eta(x, y, t). \tag{8}$$

For free surface flows with simple geometries, it is useful to represent the velocity potential, ϕ, as a sum of the homogeneous solutions of the Laplace equation. In rectangular co-ordinates, a homogeneous solution can take the form

$$\phi \sim e^{ik_x x}\, e^{ik_y y}\, e^{\pm kz}, \tag{9}$$

where $k = |\vec{k}| = \sqrt{k_x^2 + k_y^2}$ is a horizontal wavenumber. The total solution ϕ can then be written as

$$\phi(x, y, z, t) = \sum_{\vec{k}} C_{\vec{k}}^{(\pm)}(t)\, e^{ik_x x}\, e^{ik_y y}\, e^{\pm kz}, \tag{10}$$

where $C_{\vec{k}}^{(\pm)}$ is the coefficient of the $e^{ik_x x}\, e^{ik_y y}\, e^{\pm kz}$ mode. One can find solutions of the Laplace equation by finding $C_{\vec{k}}^{(\pm)}(t)$ instead of solving the Laplace equation directly. The basis functions are, in general, modified with respect to the system's symmetry. This method can be classified as one of the spectral methods [43], which are frequently used in many kinds of numerical calculations.

This kind of expansion of the velocity potential ϕ is very similar to the Stokes expansion. For example, in a two-dimensional system, the Stokes expansion is

$$\phi(x, z, t) = \sum_{k} C_k^{(\pm)}\, e^{i(kx - \omega(k)t)}\, e^{\pm kz}. \tag{11}$$

In the Stokes expansion, the coefficients are time-independent and the modes are related to space and time with their dispersion relationships. In most of the examples using the Stokes expansion in numerical calculations, the expansion would be used to find 'steady' free surface flows. In this paper, focus is on unsteady free surface motions. There has been a similar approach to unsteady motions [44]. But in that approach, a small amplitude assumption should be satisfied, so that Taylor's expansion about mean height level is used. In this paper, the coefficients can be determined without such an assumption.

Here, the coefficients $C_{\vec{k}}^{(\pm)}$ will be determined from the dynamic boundary condition. First, ϕ_t is calculated from Equation (8), and after collocating a sufficient number of ϕ_t values at different positions, the coefficients $\mathrm{d}C_{\vec{k}}^{(\pm)}/\mathrm{d}t$ are determined from the relationship between ϕ_t and $\mathrm{d}C_{\vec{k}}^{(\pm)}/\mathrm{d}t$. From the relationship between $C_{\vec{k}}^{(\pm)}$ and ϕ, one can write the relationship between $\mathrm{d}C_{\vec{k}}^{(\pm)}/\mathrm{d}t$ and ϕ_t as

$$\phi_t(x, y, z, t) = \sum_{\vec{k}} \frac{\mathrm{d}C_{\vec{k}}^{(\pm)}}{\mathrm{d}t}(t)\, e^{ik_x x}\, e^{ik_y y}\, e^{\pm kz}. \tag{12}$$

If ϕ_t is calculated at N different positions, say $x_i = i\Delta x$ for $i = 1, 2, 3, \ldots, N$, then one has N equations for ϕ_t and $\mathrm{d}C_{\vec{k}}^{(\pm)}/\mathrm{d}t$. In a simple two-dimensional case, the set of equations can be written as

$$\phi_t(x_i, \eta(x_i, t), t) = \sum_{k} \frac{\mathrm{d}C_k^{(\pm)}}{\mathrm{d}t}(t)\, e^{ikx_i}\, e^{\pm k\eta(x_i, t)}, \quad \text{for } i = 1, 2, 3, \ldots, N. \tag{13}$$

If N is equal to the number of modes used in the series expansion, the time derivatives of the coefficients $\mathrm{d}C_k^{(\pm)}/\mathrm{d}t$ can be determined, unless the equations are linearly dependent on each other. Usually, to avoid numerical instability that can arise during the coefficient determination, N is chosen to be larger than the number of modes and the differences between the right-hand side and the left-hand side of Equation (13) are minimized.

By solving N variable linear equations, Equation (13), $\mathrm{d}C_{\vec{k}}^{(\pm)}/\mathrm{d}t$ can be obtained. Simultaneously, η_t is calculated from Equation (7). Then, $C_{\vec{k}}^{(\pm)}$ and η can be updated using $\mathrm{d}C_{\vec{k}}^{(\pm)}/\mathrm{d}t$ and η_t.

Many kinds of time marching schemes can be used for updating $C_{\vec{k}}^{(\pm)}$ and η. In this paper, focus is more on the validity of the series expansion of the velocity potential than on the selection of time marching schemes. A predictor–corrector scheme is used for updating $C_{\vec{k}}^{(\pm)}$ and η. The scheme is expressed by the following equations:

$$\text{predictor: } \tilde{A}(t_0+\Delta t) = A(t_0-\Delta t) + 2\Delta t \frac{\mathrm{d}A}{\mathrm{d}t}(t_0). \tag{14}$$

$$\text{corrector: } A(t_0+\Delta t) = A(t_0) + \frac{\Delta t}{2}\left[\frac{\mathrm{d}A}{\mathrm{d}t}(t_0) + \frac{\mathrm{d}\tilde{A}}{\mathrm{d}t}(t_0+\Delta t)\right]. \tag{15}$$

Here, A represents $C_k^{(\pm)}$ or η and $\mathrm{d}\tilde{A}/\mathrm{d}t$ is the time derivative of the predicted value $\tilde{A}$. For the implementation of the predictor–corrector scheme, it is found to be more efficient to calculate $\mathrm{d}C_k^{(\pm)}/\mathrm{d}t$ than to calculate $C_k^{(\pm)}$. This time marching scheme turns out to be accurate.

Since this method is highly dependent on the system's geometry, it is difficult to generally extend this method. However, in spite of this disadvantage, this method has some merits. One of the merits is that once the coefficients are known, one can easily calculate the derivatives of ϕ, as well as its value. Also, this method may overcome one of the shortcomings of the height function method, i.e. the accuracy problem occurring when the slope of the free surface is greater than the grid resolution. This is because, in this method, there is no need to divide the space into cells in the vertical direction.

Now the time complexity of the present method is discussed. The method spends most of its computing power in solving the set of equations in Equation (13). The time complexity is nearly the same as that of the linear equation solver. If N data are collocated and N_{mode} modes are used, the time complexity of the linear equation solver can be lowered to NN_{mode}. This represents the numerical efficiency of the present method, which is comparable with those of the boundary integral method [19–21] and other methods [22–27] for an inviscid fluid. The time complexity of NN_{mode} is verified from test calculations. The computational efforts with different N and N_{mode} values are given in Table I. The values represent the times spent, which are normalized by the time spent when $N=64$ and $N_{\mathrm{mode}}=31$. The time complexity is found to be almost linear in N and N_{mode}.

Since a finite number of modes is being used in numerical calculations, it is necessary to examine the convergence of the series of Equation (10). There are some reports about the convergence of the Stokes expansion [29,30], which conclude that the convergence of the Stokes expansion is achieved when the amplitude of waves, i.e. half of the height difference between crests and troughs, is not too large. If the wave amplitude is large, one would use other techniques to improve the convergence rate, e.g. the hodograph formulation [30,45] and Padé approximants [29]. This comment may work the same on the method proposed in this section. The convergence of the present method is studied by considering surface gravity waves as a test problem with different wave amplitudes.

Table I. Computational efforts with respect to N and N_{mode}.

$N=64$							
N_{mode}	15	23	31	39	47	55	63
Efforts	0.412	0.767	1.000	1.263	1.550	1.858	2.199
$N_{\mathrm{mode}}=31$							
N	32	40	48	56	64	72	80
Efforts	0.644	0.733	0.823	0.908	1.000	1.092	1.187

The values represent the times spent, which are normalized by the time spent for $N=64$ and $N_{\mathrm{mode}}=31$. The time complexity is almost linear in N and N_{mode}.

Table II. Results of the convergence test with respect to N and N_{mode}.

		N							
		128	96	64	48	32	24	16	8
N_{mode}	95	0.2312213							
	63	0.2312213	0.2312169						
	47	0.2312213	0.2312169	0.2312041					
	31	0.2312213	0.2312169	0.2312041	0.2311864	0.2311362			
	23	0.2312213	0.2312168	0.2312041	0.2311863	0.2311361	0.2310670		
	15	0.2312177	0.2312133	0.2312008	0.2311832	0.2311336	0.2310657	0.2308892	
	7							0.2308268	0.2308891

The values are $\eta(x = 0, t = 6.28)$ with different N and N_{mode} values.

4. TEST CALCULATION AND DISCUSSION OF NUMERICAL ACCURACY

As the test problem, surface gravity waves are considered, for which the dispersion relation is given by

$$\omega \cong \omega_0 + \frac{1}{2}\epsilon^2\omega_2,$$

$$\omega_0^2 = gk \tanh kh_0,$$

$$\omega_2 = \sqrt{gk}\,(9\omega_0^{-7} - 12\omega_0^{-3} - 3\omega_0 - 2\omega_0^5)/32, \tag{16}$$

from a pertubation calculation [36]. This relationship is for the waves formed in an infinitely long tank which has a uniform depth h_0 under gravity g. Here, k is the wavenumber and ϵ is the steepness, defined as $\epsilon = ka$, where a is the wave amplitude. An easy way of confirming the accuracy of the numerical method would be to examine the dispersion relation.

Considering the boundary condition at the bottom, $z = -h_0$, the velocity potential can be written as

$$\phi(x, y, z, t) = 2\sum_{\vec{k}} C_{\vec{k}}(t)\, \mathrm{e}^{ik_x x}\, \mathrm{e}^{ik_y y}\, \mathrm{e}^{kh_0} \cosh[k(z - h_0)], \tag{17}$$

where $k = \sqrt{k_x^2 + k_y^2}$. To find the velocity potential, one just needs to determine $C_{\vec{k}}(t)$ instead of calculating ϕ itself.

The initial conditions for the problem are obtained from the approximate analytical solution of Tadjbakhsh and Keller [36] and the computed solution is compared with the approximate analytical one.

The calculation is performed in two-dimensional space. The horizontal direction is denoted by x and the vertical by z. A periodic boundary condition is imposed in the horizontal direction. The direction of gravity is downwards, $-z$-direction, and its magnitude g is normalized to 1. The width, L, is taken to be 2π and the depth, h_0, to be 3. Sixty-four data points are collocated uniformly in the whole region and 31 modes are used for the expansion. The parameters used, N and N_{mode}, are confirmed to be accurate enough by the following convergence test. The results of the convergence test are shown in Table II. The values in Table II are $\eta(x = 0, t = 6.28)$ for different N and N_{mode} values. Note that the results almost depend on N rather than N_{mode} because, in the present example, only a few modes take part in the

dynamics. The time step, Δt is set to 0.01, which is found to be within the numerical stability range.

To determine the coefficients, C_k, many kinds of methods can be used. A couple of methods have been tested. The results do not differ much from each other. In this paper, all results presented are prepared, for the determination of the coefficients, with the IMSL non-linear least square code, UNLSJ.

Figure 1 shows a temporal evolution of the free surface profile for $\epsilon = 0.05$. The horizontal direction is the x-axis and the vertical direction is the time axis. The surface profile is plotted as a three-dimensional surface with respect to space and time. In the figure, a regular periodic pulsation is shown.

In Figure 2, $\eta(x = 0, t)$ is plotted for $\epsilon = 0.05$, 0.1 and 0.2, which correspond to Figure 2(a), (b) and (c), respectively. With increasing ϵ value, non-linearity takes a more important role. The case of $\epsilon = 0.2$, which is about 45% of the Stokes limiting steepness [44], is adequately non-linear. By considering larger ϵ cases, there is confidence in the convergence of the series expansion and the validity of the method for non-linear problems. For comparison, Tadjbakhsh and Keller's approximate analytic results [36] are also plotted (represented by dashed lines). In Figure 2(a) it is hard to distinguish the numerical result from the Tadjbakhsh and Keller's series solution. As ϵ becomes larger, there are differences between the two results.

To compare the two results, i.e. the numerical result and the approximate analytical result, further, power spectrums of $\eta(x = 0, t)$ are given in Figure 3. Figure 3(a), (b) and (c) correspond to the cases of $\epsilon = 0.05$, 0.1 and 0.2, respectively. The power spectrums are obtained from the time series of $\eta(x = 0, t)$ for about 260 periods. The resolution of the power spectrum, $\Delta\omega$ is about 0.003. In Figure 3(a), the major peak is located at $\omega = 0.999$, which is

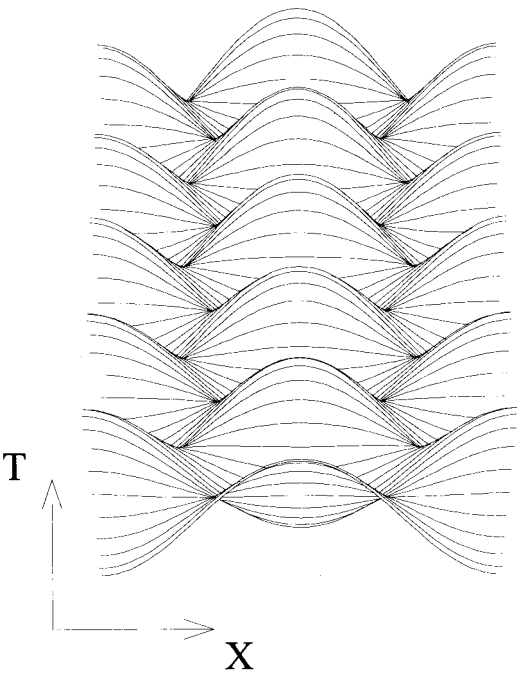

Figure 1. Temporal evolution of the free surface profile for surface gravity waves with $\epsilon = 0.05$. The horizontal axis is for space and the vertical axis is for time. A regular periodic pulsation is seen.

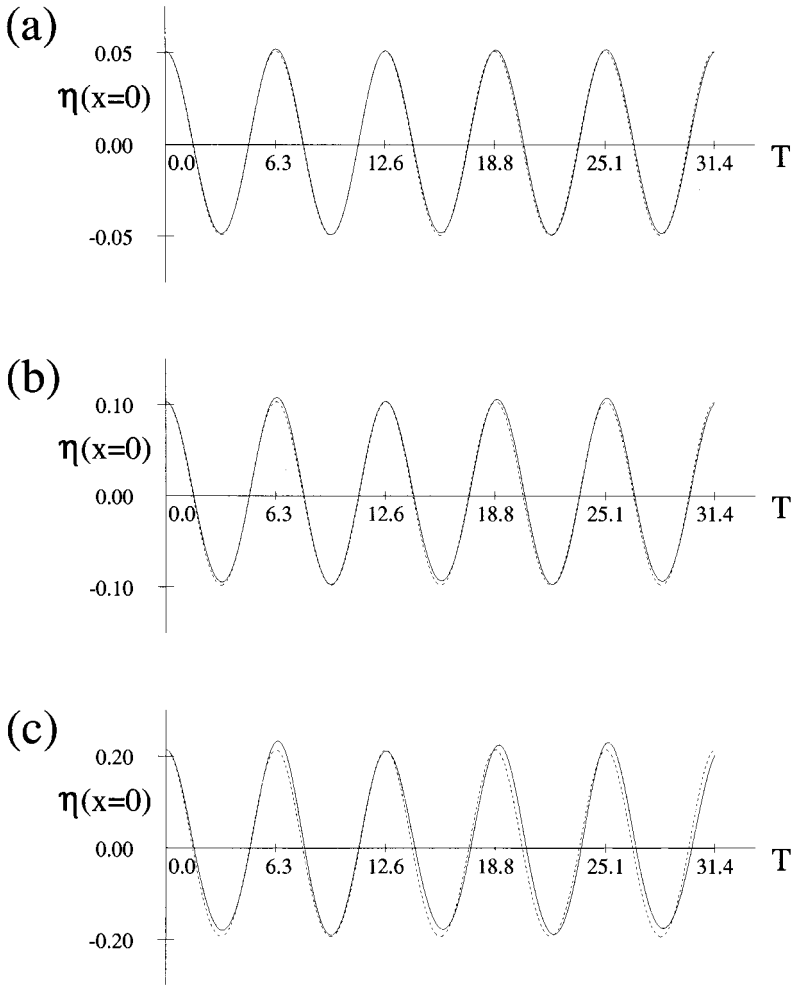

Figure 2. Time series of $\eta(x=0, t)$. (a), (b) and (c) correspond to the cases of $\epsilon = 0.05$, 0.1 and 0.2, respectively. For comparison, Tadjbakhsh and Keller's series solution is plotted by dashed lines (– – –).

nearly equal to the value, 0.997, from the dispersion relation (16) within the resolution. In this case, it is found that the time periodicity arises as the analytical studies predict and the period is nearly equal to the analytical one, even if no time periodicity is imposed. The second largest peak is the second harmonics of the major frequency and the smallest peak corresponds to the frequency for the second smallest k value, which is $\sqrt{2}$ times the major frequency. Call this frequency the second frequency. From the dispersion relation (Equation (16)), it can be found that the frequency is almost proportional to $\sqrt{k}$ when h_0 is large enough. The numerical result agrees well with the proportionality of the dispersion relation.

In Figure 3(b), for $\epsilon = 0.1$, the major frequency is 0.999 while the expected frequency from the series solution is 0.994. The amplitudes of the second harmonics and the second frequency increase. A new frequency can be seen at the location of $\sqrt{3}$ times the major frequency, the third frequency. For $\epsilon = 0.2$, the major peak shifts to 0.991 and the expected frequency from the series solution is 0.990. The amplitudes of the second frequency, the third frequency and the second harmonics of the major frequency increase further. In addition, new frequencies

appear, which are thought to correspond to the sum frequency and the difference frequency of the major frequency and the second frequency. Also, as ϵ increases further, it is observed that the major frequency broadens.

The numerical results exhibit frequency shifts, frequency broadenings and new frequency generations, which are general phenomena in non-linear wave interactions. This paper considers that the numerical results are more realistic than the series solutions that were obtained by imposing a time periodicity.

Next, the mass conservation is examined. This is another way to confirm the validity of a numerical method. Consider a temporal variation of the average height of the free surface, which is equivalent to the temporal variation of volume or mass. From the results, it can be found that the value stays at zero for about 300 wave periods.

Note that an extension of the present method to three-dimensional problems is straightforward. To achieve the same order of accuracy, if N and N_{mode} are used in two-dimensional

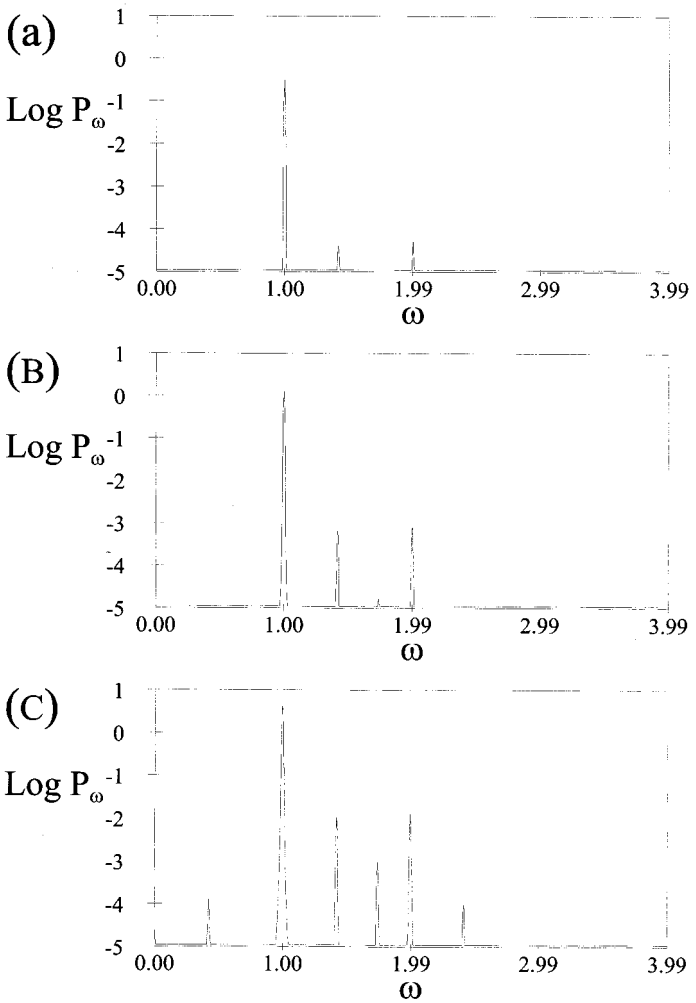

Figure 3. Power spectrums of $\eta(x = 0, t)$. (a), (b) and (c) correspond to the cases of $\epsilon = 0.05$, 0.1 and 0.2, respectively. As ϵ increases, frequency shifts, frequency broadenings and new frequency generations appear.

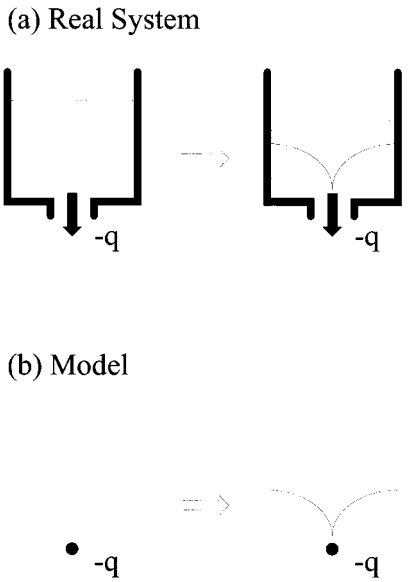

Figure 4. Schematic drawing for a dip formation in (a) a real system and (b) a simplified model.

calculations, N^2 and N_{mode}^2 should be used in three-dimensional calculations. Since the computational cost is proportional to NN_{mode} in two-dimensional calculations, it is proportional to $N^2N_{\text{mode}}^2$ in three-dimensional calculations. Considering the time complexity and the computing power available, the present method seems suitable for three-dimensional calculations. Examples of three-dimensional calculations with the present method can be found elsewhere [46].

5. APPLICATION TO A SINK FLOW WITH A FREE SURFACE

The present method appears applicable to non-linear wave interaction problems. However, in this paper, the method is applied to a more interesting problem, a dip formation. A dip formation is one of the interesting surface flow phenomena that is found frequently, e.g. in selective withdrawal problems [47–52] and in gas entrainment problems in nuclear reactors [53–59]. In spite of its wide applicability, not much is known because of the difficulty in approaching the problem. Applying the numerical method to this problem is an example for simplified models, which can be studied instead of the complicated original systems.

There are several topics on the study of dip formation problems. Steady state solutions are usually studied [60–65]. However, not many works have been reported about the temporal evolutions of the free surface. Focus is on the evolutions of the free surface profile. To compare the results, the results of Tyvand's series solutions for a line sink [39] are used.

Free surface flows occurring when fluid flows out through a hole at the bottom of a tank, can be treated by free surface flows due to a sink which is located in a semi-infinite fluid (Figure 4). A line sink is considered, which is located at $(0, -H)$. The volume flux is Q_0. Initially, the free surface profile is $\eta = 0$ and the internal velocity potential is 0 everywhere, which can be imposed by letting all $C_{\bar{k}}$ be zero. At $t = 0$, the sink is turned on and the free surface profile changes due to the sink effect and gravity. Dimensionless quantities are

introduced by defining H as a unit of length, $\sqrt{gH^3}$ as unit a of volume flux and velocity potential, and $\sqrt{H/g}$ as a unit of time. Through this non-dimensionalization, the governing equations become Equations (6)–(8), with $g = 1$.

Considering the sink effect, the governing equation becomes a Poisson equation,

$$\nabla^2\phi = q(\vec{x}), \tag{18}$$

with proper boundary conditions. Here, $q(\vec{x})$ is a function due to the sink. If a volumeless sink is considered, the function $q(\vec{x})$ can be written as

$$q(\vec{x}) = q_0\delta(\vec{x} - \vec{x}_0), \tag{19}$$

where $\vec{x}_0$ is the location of the sink and q_0 is the strength of the sink. Since a semi-infinite fluid is considered, the boundary condition at $z \to -\infty$ is used instead of the boundary condition at the bottom. The boundary condition is written as

$$|\nabla\phi| \to 0 \quad \text{as} \quad z \to -\infty. \tag{20}$$

The other boundary conditions do not change although a sink exists.

To find solutions of the Poisson equation, the steps of Tyvand's calculations [39] are followed, where the velocity potential is written as a sum of an external singular velocity potential due to the sink, ϕ_e and an internal velocity potential, ϕ_i.

$$\phi = \phi_e + \phi_i. \tag{21}$$

The external velocity potential and the internal velocity potential satisfy the following Poisson equation and Laplace equation, respectively.

$$\nabla^2\phi_e = q_0\delta(\vec{x} - \vec{x}_0), \tag{22}$$

$$\nabla^2\phi_i = 0. \tag{23}$$

It should be noted that the boundary conditions must be satisfied by the total velocity potential.

The Poisson equation can often be solved with the image source method for the systems with simple geometries. If the free surface elevation is constant, i.e. $\eta(x, y) = \text{constant}$, the external velocity potential will be the sum of the velocity potential due to the sink, which is regarded as a sink located in an infinite fluid, and the velocity potential of its mirror image. For a line sink of strength q_0, which is located at $(0, -h_0)$ in x–z-plane, the external potential is written by

$$\phi_e = \frac{q_0}{4\pi}\log[x^2 + (z + h_0)^2] + (\text{image term}). \tag{24}$$

The above expression for the external velocity potential can be used as an assumption for calculations of dip formations. This assumption is valid when the surface distortion is not too large. Numerical solutions of dip formation problems are sought using the above external velocity potential assumption.

Since the internal velocity potential should satisfy the Laplace equation under proper boundary conditions, an efficient method is needed to solve the Laplace equation. The present numerical method is applied to this problem. Considering the boundary condition at $z \to -\infty$, the internal velocity potential can be written as

$$\phi_i(x, y, z, t) = \sum_{\vec{k}} C_{\vec{k}}(t)\, e^{ik_x x}\, e^{ik_y y}\, e^{kz}. \tag{25}$$

In this paper, two-dimensional cases are only considered. Considering symmetry, only the even modes are used in the expansion, and calculations are performed in the right-half space. Data at 65 points are sampled to determine 32 mode coefficients. The width of the whole region is 10, so that the width of the calculational region is 5. The time step, Δt, is taken to be 0.001, which is smaller than the Δt used in the previous section because dip formation phenomena usually exhibit drastic changes in the surface profile. To determine the coefficients, the IMSL non-linear least square routine is used.

Figures 5 and 6 are the numerical results for the sinks whose strengths are 1.8 and 0.2, respectively. Free surface profiles calculated numerically at different times are drawn with solid lines. Free surface profiles are plotted only in the half region considering the symmetry. The time intervals between the nearest free surface profiles are 0.02 in Figure 5 and 0.2 in Figure 6. For $q_0 = 1.8$, the sink strength is large enough so that the free surface moves downwards and a dip forms. However, for $q_0 = 0.2$, the sink strength is not sufficiently large for a dip to form. The free surface moves downwards for a while after the sink is turned on, but soon after, the free surface moves upwards because gravitational restoration dominates the sink effect.

Tyvand's series solutions are drawn with dashed lines in Figure 6, for the same condition of the numerical calculations. The series solutions for $q_0 = 1.8$ are not plotted because the results are too close to the numerical results to distinguish between the two results in the resolution of the figure. Instead, for a comparison of the two results, the free surface locations at some x positions are shown in Table III. The data correspond to the last, i.e. the lowest, surface profile in Figure 5. The differences between the two results are only about 10^{-5}.

Also found is that for $q_0 = 0.2$, the numerical results agree well with the series solutions for small t. But as time evolves, the two results exhibit disagreements. The main reason for the disagreements is that the numerical calculations were performed in a practical finite domain, whereas the series solutions were obtained in a hypothetical infinite domain. It is shown in Figure 6 that the numerical results are smaller than the series solutions', near the end of the calculational domain. In the series solutions, fluid supply from outside of the domain is due to

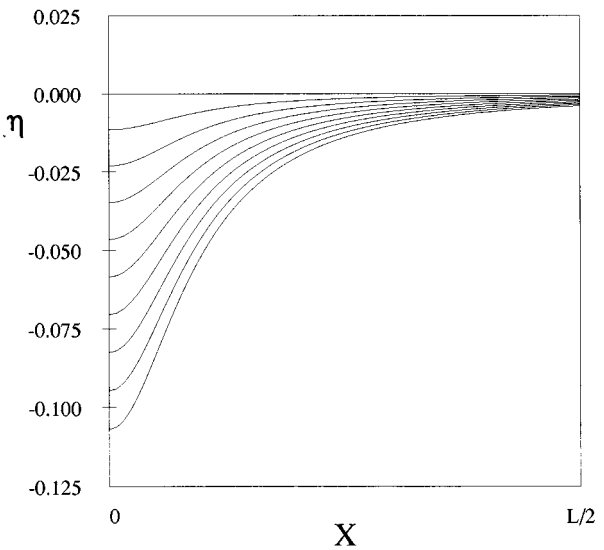

Figure 5. Evolution of the free surface profile due to a line sink of strength $q_0 = 1.8$. The free surface moves downwards and a dip is about to form. The time intervals between the nearest surface profiles are 0.02.

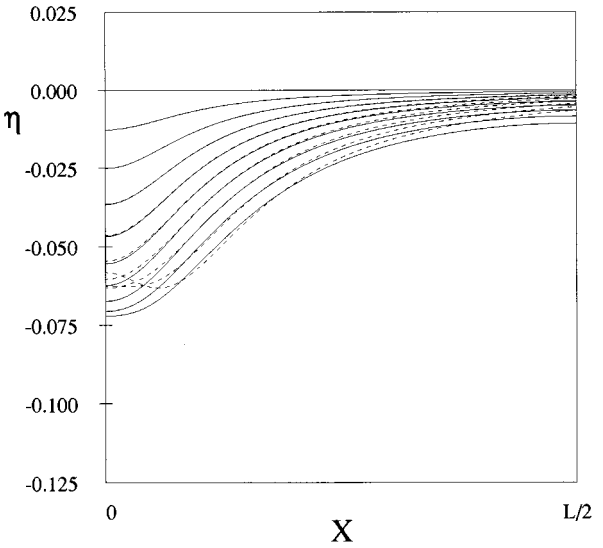

Figure 6. Evolution of the free surface profile due to a line sink of strength $q_0 = 0.2$. The numerical results are drawn with solid lines (—) and Tyvand's series solutions are drawn with dashed lines (– – –). The time intervals between the nearest surface profiles are 0.2. In the series solutions, for a while after the sink is turned on, the free surface moves downwards, but soon the free surface moves upwards because gravitational restoration dominates the sink effect.

both the internal and the external velocity potential, while in the numerical calculations, fluid supply is actually due to the external velocity potential, i.e. the sink effect. Because of the disagreements near the end of the domain, the slopes of the series solutions are greater than the slopes of the numerical results. This makes gravitational restoration of the series solutions larger than that of the numerical results. Thus, the free surface moves upwards more quickly for the series solutions.

In short, the disagreements can be explained by the effect of the finiteness of the domain. For infinite fluids, the mean height of the free surface does not change in time. But for finite fluids, the mean height decreases as time goes on. This is the main difference between infinite and finite fluids. A recent investigation reported that gravitational effects were larger for infinite fluids than for finite fluids [40]. This comment agrees well with the numerical results presented in this paper.

Table III. Comparison between the numerical results and the series solutions.

X position (L)	Series solution	Numerical results
0	-1.06975×10^{-1}	-1.06959×10^{-1}
1/16	-7.41286×10^{-2}	-7.40894×10^{-2}
1/8	-3.95611×10^{-2}	-3.95352×10^{-2}
3/16	-2.24578×10^{-2}	-2.24283×10^{-2}
1/4	-1.40188×10^{-2}	-1.39866×10^{-2}
5/16	-9.45742×10^{-3}	-9.42230×10^{-3}
3/8	-6.76775×10^{-3}	-6.72896×10^{-3}
7/16	-5.06564×10^{-3}	-5.02231×10^{-3}
1/2	-3.92638×10^{-3}	-3.88459×10^{-3}

Data correspond to the lowest surface profile in Figure 5. The differences are only about 10^{-5}.

The above arguments can explain the disagreements for $q_0 = 0.2$. However, new questions arise. Why does the disagreement appear only for $q_0 = 0.2$? What is the difference between $q_0 = 1.8$ and $q_0 = 0.2$? Before answering the questions, one should think about how the finite size effect influences the dynamics. The free surface near the center can not perceive whether the domain is finite or infinite, unless there is an interaction between the center where the dip formation occurs and the end of the domain. At the end of the domain, the surface does not distort before waves formed at the center arrive. The waves arrive at the end of the domain and they are reflected back. These reflected waves affect the surface profile near the center. Briefly, the finite size effect influences the dynamics through the waves that travel back and forth. Now, the questions will be answered. The answer involves the time scale taken for the waves to arise, travel to the end of the domain, be reflected back and carry the information about the end of the domain to the center. The time scale is nearly the same, whatever q_0 is. It mainly depends on the length of the domain. There is not enough time for the finite size effect influences the surface profile when q_0 is large, while the effect plays an important role in the dynamics when q_0 is small. In some numerical calculations of an infinite domain with a finite domain, the calculations were only performed until the waves did not arrive at the end of the domain [26].

From the above results, it is concluded that the present numerical method accurately describes the phenomena, in spite of the singular nature of a sink. Especially for small t, the numerical results can not be distinguished from the series solutions. This is a remarkable result. This also guarantees the series expansion of velocity potential converges well for the cases considered here.

6. CONCLUDING REMARKS

In this study, a numerical method suitable for free surface flows is proposed. A free surface is represented by a height function and the governing equations for the free surfaces, under the assumption of a potential flow, are reduced to a Laplace equation with proper boundary conditions. The solutions of the Laplace equation are written in terms of a sum of the linear homogeneous solutions and the coefficients of the homogeneous eigensolutions for the given boundary conditions are then determined at all time steps, which determines the motion of the unsteady free surfaces.

The present method was applied to surface gravity waves and it was found that the accuracy and the time complexity, even though the method is simple, are comparable with those of well-established methods. A dip formation problem was considered as an example of the application. The results were nearly equal to the approximate solutions. In conclusion, the present method is efficient for free surface flows with simple geometries.

ACKNOWLEDGMENTS

The authors are thankful for the support in part by the Korea Science and Engineering Foundation, in part by KAIST and in part by the Korea Atomic Energy Research Institute.

REFERENCES

1. C.W. Hirt and B.D. Nichols, 'Volume of fluid (VOF) method for the dynamics of free boundaries', *J. Comput. Phys.*, **39**, 201–225 (1981).

2. F. Mashayek and N. Ashgriz, 'A hybrid finite element–volume of fluid method for simulating free surface flows and interfaces', *Int. J. Numer. Methods Fluids*, **20**, 1363–1380 (1995).
3. F.H. Harlow and J.E. Welch, 'Numerical calculation of time-dependent viscous incompressible flow of fluid with free surface', *Phys. Fluids*, **8**, 2182–2189 (1965).
4. F.H. Harlow and J.E. Welch, 'Numerical study of large-amplitude free surface motions', *Phys. Fluids*, **9**, 842–851 (1966).
5. R.K.-C. Chan and R.L. Street, 'A computer study of finite amplitude water waves', *J. Comput. Phys.*, **6**, 68–94 (1970).
6. D.B. Johnson, P.E. Raad and S. Chen, 'Simulation of impacts of fluid free surfaces with solid boundaries', *Int. J. Numer. Methods Fluids*, **19**, 153–176 (1994).
7. P.E. Raad, S. Chen and D.B. Johnson, 'The introduction of microcells to treat pressure in free surface fluid flow problems', *J. Fluids Eng. Trans. ASME*, **117**, 683–690 (1995).
8. H. Miyata, 'Finite difference simulation of breaking waves', *J. Comput. Phys.*, **65**, 179–214 (1986).
9. I.-L. Chern, J. Glimm, O. McBryan, B. Plohr and S. Yaniv, 'Front tracking for gas dynamics', *J. Comput. Phys.*, **62**, 83–110 (1986).
10. S.O. Unverdi and G. Tryggvason, 'A front-tracking method for viscous, incompressible, multifluid flows', *J. Comput. Phys.*, **100**, 25–37 (1992).
11. S.O. Unverdi and G. Tryggvason, 'Computations of multifluid flows', *Physica D*, **60**, 70–83 (1992).
12. C.W. Hirt, J.L. Cook and T.D. Butler, 'A Lagrangian method for calculating the dynamics of an incompressible fluid with free surface', *J. Comput. Phys.*, **5**, 103–124 (1970).
13. G. Ryskin and L.G. Leal, 'Numerical solution of free boundary problems in fluid mechanics. Part 1. The finite difference technique', *J. Fluid. Mech.*, **148**, 1–17 (1984).
14. J.M. Hyman, 'Numerical methods for tracking interfaces', *Physica D*, **12**, 396–407 (1984).
15. H. Liu and M. Ikehata, 'Computation of free surface waves around an arbitrary body by a Navier–Stokes solver using the pseudo-compressibility technique', *Int. J. Numer. Methods Fluids*, **19**, 395–413 (1994).
16. N.S. Asaithambi, 'Computation of free-surface flows', *J. Comput. Phys.*, **73**, 380–394 (1987).
17. M.J. Fritts and J.P. Boris, 'The Lagrangian solution of transient problems in hydrodynamics using a triangular mesh', *J. Comput. Phys.*, **31**, 173–215 (1979).
18. P. Bach and O. Hassager, 'An algorithm for the use of the Lagrangian specification in Newtonian fluid mechanics and applications to free surface flow', *J. Fluid Mech.*, **152**, 173–190 (1985).
19. G.R. Baker, D.I. Meiron and S.A. Orszag, 'Boundary integral methods for axisymmetric and three-dimensional Rayleigh–Taylor instability problems', *Physica D*, **12**, 19–31 (1984).
20. D.G. Dommermuth and D.K. Yue, 'Numerical simulations of non-linear axisymmetric flows with a free surface', *J. Fluid Mech.*, **178**, 195–219 (1987).
21. Q.-N. Zhou and W.P. Graebel, 'Axisymmetric draining of a cylindrical tank with a free surface', *J. Fluid Mech.*, **221**, 511–532 (1990).
22. S.J. Zaroodny and M.D. Greenberg, 'On a vortex sheet approach to the numerical calculation of water waves', *J. Comput. Phys.*, **11**, 440–446 (1973).
23. G.R. Baker, D.I. Meiron and S.A. Orszag, 'Vortex simulations of the Rayleigh–Taylor instability', *Phys. Fluids*, **23**, 1485–1490 (1980).
24. G.R. Baker, D.I. Meiron and S.A. Orszag, 'Generalized vortex methods for free surface flow problems', *J. Fluid Mech.*, **123**, 477–501 (1982).
25. J.G. Telste, 'Potential flow about two counter-rotating vortices approaching a free surface', *J. Fluid Mech.*, **201**, 259–278 (1989).
26. E.M. Sozer and M.D. Greenberg, 'The time-dependent free surface flow induced by a submerged line source or sink', *J. Fluid Mech.*, **284**, 225–237 (1995).
27. G. Tryggvason, 'Numerical simulations of the Rayleigh–Taylor instability', *J. Comput. Phys.*, **75**, 253–282 (1988).
28. G.B. Whitham, *Linear and Non-linear Waves*, Wiley, New York, 1974.
29. J.Y. Holyer, 'Large amplitude progressive interfacial waves', *J. Fluid Mech.*, **93**, 433–448 (1979).
30. P.G. Saffman and H.C. Yuen, 'Finite amplitude interfacial waves in the presence of a current', *J. Fluid Mech.*, **123**, 459–476 (1982).
31. M.M. Rienecker and J.D. Fenton, 'A Fourier approximation method for steady water waves', *J. Fluid Mech.*, **104**, 119–137 (1981).
32. P.J. Bryant, 'Cyclic gravity waves in deep water', *J. Aust. Math. Soc. Ser. B*, **25**, 2–15 (1983).
33. P.J. Bryant, 'Oblique wave groups in deep water', *J. Fluid Mech.*, **146**, 1–20 (1984).
34. P.J. Bryant, 'Doubly periodic progressive permanent waves in deep water', *J. Fluid Mech.*, **161**, 27–42 (1985).
35. P.J. Bryant, 'Non-linear progressive free waves in a circular basin', *J. Fluid Mech.*, **205**, 453–467 (1989).
36. I. Tadjbakhsh and J.B. Keller, 'Standing surface waves of finite amplitude', *J. Fluid Mech.*, **8**, 442–451 (1960).
37. Q.-N. Zhou and W.P. Graebel, 'Free surface oscillations in a slowly draining tank', *ASME J. Appl. Mech.*, **59**, 438–444 (1992).
38. B.T. Lubin and G.S. Springer, 'The formation of a dip on the surface of a liquid draining from a tank', *J. Fluid Mech.*, **29**, 385–390 (1967).
39. P.A. Tyvand, 'Unsteady free surface flow due to a line source', *Phys. Fluids A*, **4**, 671–676 (1992).

40. H. Miloh and P.A. Tyvand, 'Non-linear transient free surface flow and dip formation due to a point sink', *Phys. Fluids A*, **5**, 1368–1375 (1993).
41. L.K. Forbes and G.C. Hocking, 'The bath-plug vortex', *J. Fluid Mech.*, **284**, 43–62 (1995).
42. B.D. Nichols and C.W. Hirt, 'Improved free surface boundary conditions for numerical incompressible flow calculations', *J. Comput. Phys.*, **8**, 434–448 (1971).
43. C. Canuto, M.Y. Hussaini, A. Quarteroni and T.A. Zang, *Spectral Methods in Fluid Dynamics*, Springer, New York, 1988.
44. D.G. Dommermuth and D.K.P. Yue, 'A high-order spectral method for the study of non-linear gravity waves', *J. Fluid Mech.*, **184**, 267–288 (1987).
45. V. Bontozoglou, S. Kallidasis and A.J. Karabelas, 'Inviscid free surface flow over a periodic wall', *J. Fluid Mech.*, **226**, 189–203 (1991).
46. H.Y. Nam, *et al.*, *Liquid Metal Reactor Development: Development of LMR Coolant Technology*, KAERI/RR-1690/96, 1997.
47. H.P. Pao and T.W. Kao, 'Dynamics of establishment of selective withdrawal of a stratified fluid from a line sink. Part 1. Theory', *J. Fluid Mech.*, **65**, 657–688 (1974).
48. J. Imberger, R.O.R.Y. Thompson and C. Fandry, 'Selective withdrawal from a finite rectangular tank', *J. Fluid Mech.*, **78**, 489–512 (1976).
49. P.J. Bryant and I.R. Wood, 'Selective withdrawal from a layered fluid', *J. Fluid Mech.*, **77**, 581–591 (1976).
50. G.N. Ivey and S. Blake, 'Axisymmetric withdrawal and inflow in a density stratified container', *J. Fluid Mech.*, **161**, 115–137 (1985).
51. B.R. Munson, M.S. Ingber and P. Razifard, 'The effect of a moving sink on selective withdrawal from a discretely stratified fluid', *Phys. Fluids*, **31**, 2720–2722 (1988).
52. T.J. Singler and J.F. Geer, 'A hybrid perturbation Galerkin solution to a problem in selective withdrawal', *Phys. Fluids A*, **5**, 1156–1166 (1993).
53. M.R. Baum and M.E. Cook, 'Gas entrainment at the free surface of a liquid: entrainment inception at a vortex with an unstable gas core', *Nucl. Eng. Des.*, **32**, 239–245 (1975).
54. M. Takahashi, A. Inoue, M. Aritomi, Y. Takenaka and K. Suzuki, 'Gas entrainment at free surface of liquid, (I)', *J. Nucl. Sci. Technol.*, **25**, 131–142 (1988).
55. M. Takahashi, A. Inoue, M. Aritomi, Y. Takenaka and K. Suzuki, 'Gas entrainment at free surface of liquid, (II)', *J. Nucl. Sci. Technol.*, **25**, 245–253 (1988).
56. H. Madarame and T. Chiba, 'Gas entrainment inception at the border of a flow-swollen liquid surface', *Nucl. Eng. Des.*, **120**, 193–201 (1990).
57. G. Govindaraj, C. Raju, R.D. Kale and G. Vaidyanathan, 'Gas entrainment in surge tank of liquid metal fast breeder reactors', *J. Nucl. Sci. Technol.*, **30**, 712–716 (1993).
58. Y. Eguchi and N. Tanaka, 'Experimental study on scale effect on gas entrainment at free surface', *Nucl. Eng. Des.*, **146**, 363–371 (1994).
59. Y. Eguchi, K. Yamamoto, T. Funada, N. Tanaka, S. Moriya, K. Tanimoto, K. Ogura, T. Suzuki and I. Maekawa, 'Gas entrainment in the IHX vessel of top-entry loop-type LMFBR', *Nucl. Eng. Des.*, **146**, 373–381 (1994).
60. J.M. Vanden-Broeck and J.B. Keller, 'Free surface flow due to a sink', *J. Fluid Mech.*, **175**, 109–117 (1987).
61. E.O. Tuck and J.M. Vanden-Broeck, 'A cusp-like free surface flow due to a submerged source or sink', *J. Aust. Math. Soc. Ser. B*, **25**, 443–450 (1984).
62. G.C. Hocking, 'Cusp-like free surface flows due to a submerged source or sink in the presence of a flat or sloping bottom', *J. Aust. Math. Soc. Ser. B*, **26**, 470–486 (1985).
63. G.C. Hocking, 'Supercritical withdrawal from a two-layer fluid through a line sink', *J. Fluid Mech.*, **297**, 37–47 (1995).
64. L.K. Forbes, 'An algorithm for 3D free surface problems in hydrodynamics', *J. Comput. Phys.*, **82**, 330–347 (1989).
65. L.K. Forbes and G.C. Hocking, 'Flow caused by a point sink in a fluid having a free surface', *J. Aust. Math. Soc. Ser. B*, **32**, 231–249 (1990).

